iScience

CellPress
OPEN ACCESS

Article

Blink-sensing glasses: A flexible iontronic sensing wearable for continuous blink monitoring

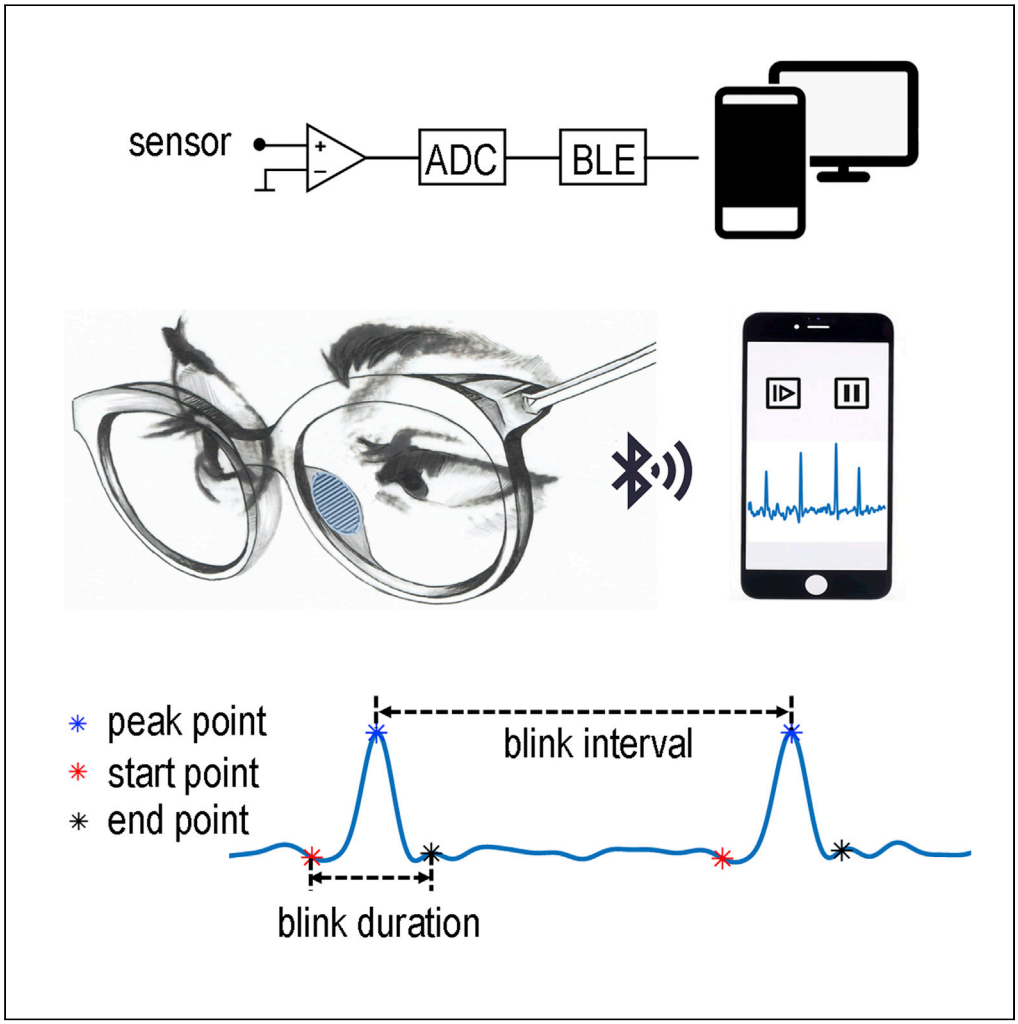

Rui Chen, Zhichao Zhang, Ka Deng, ..., Li Cai, Chi-wei Chang, Tingrui Pan

tingrui@ucdavis.edu

Highlights

Blink-sensing glasses can capture blink patterns with clinical-grade high accuracy

A FITS sensor is applied to monitor the blink by detecting the muscle movement

Blink-sensing glasses can be of potential use to prognose the dry eye

The glasses are a continuous detection manner with immunity to ambient lights

Chen et al., iScience 24, 102399
May 21, 2021 © 2021
https://doi.org/10.1016/j.isci.2021.102399

iScience

CellPress
OPEN ACCESS

Article

Blink-sensing glasses: A flexible iontronic sensing wearable for continuous blink monitoring

Rui Chen,[1,2,10] Zhichao Zhang,[3,6,10] Ka Deng,[1,7,10] Dahu Wang,[4] Hongmin Ke,[5] Li Cai,[5] Chi-wei Chang,[1] and Tingrui Pan[1,3,7,8,9,11,*]

SUMMARY

Blink reflex has long been considered closely related to physiological states, from which abundant information on ocular health and activities can be revealed. In this study, a smart glasses wearable has been developed, incorporating a flexible and sensitive pressure sensor, to monitor blink patterns by continuously detecting ocular muscular movements, referred to as blink-sensing glasses. By applying the emerging flexible iontronic sensing (FITS) sensor with the sensitivity of 340 pF/mmHg, the skin pressure variations induced by movements of the orbicularis oculi muscles can be monitored in real time. The blink-sensing glasses can successfully capture blink patterns with a high accuracy of 96.3% and have been used to differentiate the blink features from both dry-eye subjects and healthy controls. This device can be potentially used as a new clinical and research monitoring tool for continuous eye blink analysis, while providing patients with high comfortableness in long-term ambulatory and home settings.

INTRODUCTION

As an essential self-protection function of the eye, blink, also known as blink reflex clinically, has attracted considerable attention in both medical research and healthcare over the past decade. In particular, normal patterns of cyclic blinks with regular intervals are not only important to maintain ocular health but also reflect physiological conditions of the central nervous system (Aristea et al., 2014; Katsarava et al., 2010). However, blink patterns can be affected by multiple complicated factors, such as environmental stimuli (Anat et al., 2014), disease progression (Karson et al., 1984; Geyer and Braff, 2010), cognitive functions (Bryant and Lorenza, 2016), psychological and emotional states (Vermeulen et al., 2009) etc. Therefore, certain eye diseases (such as dry eye and blepharospasm) as well as physiological states (such as fatigue and attention) have been investigated to reveal their strong correlation with the periodic features of blinks (Stern et al., 1994; Jacobsen, 1996; Wang et al., 2018). For instance, several clinical studies have been carried out between groups of dry-eye patients and healthy volunteers over a period of time. These results have suggested appreciable differences present in blink rates (Kazuo, 1998; Tsubota et al., 1996; Hamrah and Foulks, 2005), blink durations (Tsubota et al., 1996), and blink intervals along with other features between the two groups (Hamrah and Foulks, 2005; Rodriguez et al., 2013). Blink detection has also been applied to monitor driving safety due to the strong correlation presented between blink patterns and fatigue levels. By different means of tracking, the eyelid movements of drivers have been recorded and analyzed, from which the blink rates and eyelid closure time can be used to correlate with the drivers' fatigue levels, as a safety feature and reminder (Jürgen et al., 2017; Taner et al., 2010). Although the above studies have shown interesting and promising results in blink analysis for understanding causes of eye diseases and monitoring physiological states of the ocular and central nervous systems, the long-term monitoring capacity is still called for, which can be used to collect extensive clinical data and derive conclusive results for such purposes (Li et al., 2012; Rodriguez et al., 2016).

A number of efforts have been attempted toward providing a high-precision blink-monitoring gadget to satisfy the unmet clinical demand, which can be categorized into either a wearable or a non-wearable approach. Specifically, optical imaging has been frequently sought to record and analyze blink patterns in a non-wearable format. For clinical applications, an ocular surface interferometer, Lipiview, is based on a high-definition camera to detect the tear film reflection on the ocular surface under illumination of

[1]Institute of Biomedical and Health Engineering, Shenzhen Institute of Advanced Technology, Chinese Academy of Sciences, Shenzhen 518055, China

[2]School of Computer Science, University of Chinese Academy of Sciences, Beijing 100049, China

[3]Micro-Nano Innovations (MiNI) Laboratory, Department of Biomedical Engineering, University of California, Davis, CA 95616, USA

[4]Department of Ophthalmology, LongHua Hospital Shanghai University of Traditional Chinese Medicine, Shanghai 200032, China

[5]Department of Ophthalmology, Shenzhen University General Hospital, Shenzhen University Clinical Medical Academy, Shenzhen 518055, China

[6]TacSense, Inc., Woodland, CA 95776, USA

[7]Shenzhen Engineering Laboratory of Single-molecule Detection and Instrument Development Shenzhen 518055, China

[8]Suzhou Institute for Advanced Research, University of Science and Technology of China, Suzhou 215123, China

[9]Department of Precision Machinery and Precision Instrumentation, University of Science and Technology of China, Hefei 230026, China

[10]These authors contributed equally

[11]Lead contact

*Correspondence: tingrui@ucdavis.edu

https://doi.org/10.1016/j.isci.2021.102399

Table 1. Comparison of methods

	Blink-sensing glasses	Infrared sensor	Contact lenses	HD camera	HD camera	Micro camera	Physiological signal detection
Reference	This study	(Dementyev and Holz, 2017)	(Faschinger and Mossbck, 2010)	Lipiview (clinical use)	(Fogelton and Benesova, 2018)	(Taner et al., 2010)	(Wu et al., 2013)
Published year	2020	2017	2010	Unknown	2018	2010	2013
Detecting method	Noninvasive	Noninvasive	Intrusive	Noninvasive	Noninvasive	Noninvasive	Noninvasive
System size	Small	Small	Small	Large	Large	Medium	Large
System complexity	Simple	Simple	Complex	Complex	Complex	Complex	Complex
Data type	Digit	Digit	Digit	Video	Video	Video	Digit
Power consumption	Low	Low	Unknown	High	High	Medium	High
Wearability	Good	Good	Good	Poor	Poor	Good	Poor
Health hazard potential	Low	Medium	High	Low	Low	Low	Low
Environmental influence	Low	High	Low	High	High	High	Low
Individual adaptability	Medium	Low	High	Low	Low	Low	High

a white light source, while indirectly measuring the blink patterns (Korb et al., 2017). Moreover, bioelectric signals, such as electroencephalogram (EEG) (Chambayil et al., 2010; Yi et al., 2010), electrooculography (EOG) (Wu et al., 2013), and electromyography (EMG) (Silverstein and Graham, 2010; Shahani, 1970), have also been utilized in clinical settings to correlate blink patterns indirectly. For instance, EOG is typically utilized to diagnose retinal diseases, in which blink signals can also be clearly distinguished and extracted (Wu et al., 2013). As a synergistic action of the orbicularis oculi muscle and the levator muscle of the upper eyelid, blink has been long detected by periorbital EMG electrodes with high precision (Silverstein and Graham, 2010), which becomes a clinical standard to diagnose ocular muscular dysfunctions (Yi et al., 2013). Unfortunately, most of the clinical-grade monitoring equipment is not designed to be wearable or miniaturizable, which limits their usage to short-term blink analyses in a highly confined environment. A recent technological trend moves toward miniaturizing the existing approaches and reformatting them into a long-term wearable fashion for continuous monitoring (Pan and Xu, 2014; Lin et al., 2020; Tsikriteas et al., 2020; Wang et al., 2020). In 2017, a research team from Microsoft has developed an eyeglass device that monitors blink rates and intervenes abnormal blink patterns for dry-eye prevention (Dementyev and Holz, 2017). It has been equipped with an infrared proximity sensor, which monitors eyelid movements and subsequently analyzes the blink rates in real time, and the patterns of blink can then be used to differentiate between normal and diseased conditions. Notably, the infrared sensor adopted in this study has the advantage of a small footprint and can be fully embedded into the existing glass frame, turning it into a truly wearable gadget. However, it meets inherent challenges, such as unavoidable influence from ambient light variations and potential harm to the retina by its continuous infrared radiation (Wolbarsht, 1980). Motion artifacts can be another challenging source of interference. In addition, the blink signals can also be substantially affected by the differences in individual facial topologies and the personalized ways that the glasses are worn (Frigerio et al., 2014). Table 1 summarizes and compares the recent works on the eye blink-sensing technologies in terms of system size, complexity, data types, power consumptions, wearability, health hazard potential, environmental impact, and individual adaptability. In conclusion, a long-term monitoring wearable with reliable analytical capacity of blink features and a safety consideration to the eye can be highly desired to collect the valuable data uninterruptedly from the patients through their daily lives.

In this work, we have proposed a flexible blink-sensing glasses system equipped with highly sensitive pressure sensors to continuously monitor the muscular movements directly related to the blink reflex, which is framed into the regular eye glasses as a truly wearable device. Benefiting from the highly sensitive and

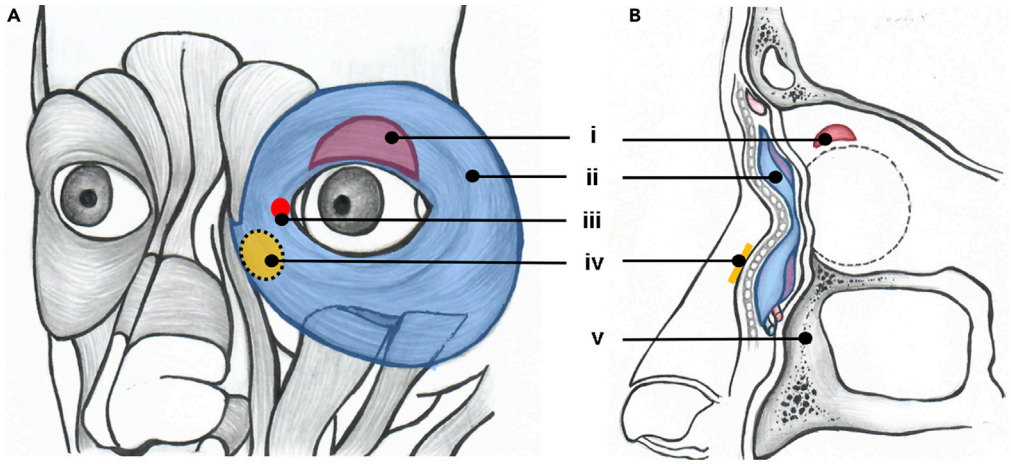

Figure 1. Measurement principle

(A) Anatomical structure of the eye muscles, with the orbicularis oculi muscle (highlighted in blue) (ii) and the levator superioris muscle (i) (highlighted in red), both of which control the blink movements. The red dot indicates the inner canthus angle (iii).

(B) The section parallel to the nose pad. (iv) The sensor placement position and (v) the maxilla.

miniature construct of the flexible iontronic sensors, the sensing unit can be integrated to the nose pads of the glasses frame, which is in direct contact with one of the main muscular bundles, i.e., orbicularis oculi muscle, controlling the eyelid movements (Shahani, 1970). We have fully characterized the pressure change recorded on the nose pad correlated with the muscular motions using a manometry approach. Accordingly, a flexible iontronic sensor (FITS) has then been designed and fabricated to track such variations in the skin pressure within a thin and flexible package (of 180 μm). It has been optimized with the device sensitivity of 340 pF/mmHg within the measurement range from 2 mmHg to 35 mmHg. In order to validate the performance of the muscular sensing from the wearable sensing glasses, we have collected and analyzed the signals in comparison with these from the clinical video standard. As a demonstration of its utility, the blink-sensing glasses have been applied to continuously track the blink features between dry-eye patients and healthy volunteers in an IRB-approved study, from which in blink rates, average blink durations and maximum blink intervals have been recorded, analyzed, and compared, and the findings have been highly consistent with the prior studies conducted in the more restricted environments. In brief, the proposed blink-sensing glasses, by offering a long-term monitoring capacity within its flexible and comfortable wearable packaging, can be highly valuable to the patients whose health data can be continuously collected and analyzed for potential diagnostic and therapeutic values in an unnoticeable and uninterrupted manner throughout their regular daily activities.

Working principle

Measurement principle

As aforementioned, blink patterns are primarily controlled by the synergistic actions of both orbicularis oculi and levator palpebrae superioris muscles. As shown in Figure 1A, the orbicularis oculi muscle (ii), a superficial facial muscle located between the subcutaneous tissue and the tarsal plate, consists of a ring-shaped muscle-fibrous tissue surrounding the orbital and palpebral fissures. Its main function is to close the eyelid, innervated by the facial nerve (Lai, 2001), whereas the levator palpebrae superioris muscle (i), innervated by the oculomotor nerves, is mainly used to raise the eyelid. For each blink cycle, as the orbicularis oculi muscle relaxes, the levator palpebrae superioris muscle contracts, and as a result, the upper eyelid opens. Subsequently, when the levator palpebrae superioris muscle relaxes, the upper eyelid closes by contracting the orbicularis oculi muscle (Lai, 2001; Mller, 1991). In brief, the blink cycles represent the repetitive process to pull eyelids alternatively by these two muscle bundles. More importantly, part of orbicularis oculi muscle stays right underneath the nose pad (iv) of the typical glasses, of which the contraction and relaxation can cause appreciable variations in skin pressure, as illustrated in Figure 1B. Specifically, during each blink, the orbicularis oculi muscles are innervated to contract, and the cross-sectional area of the muscle bundle has been altered, as supported by the maxilla (v) skeletal structure underneath, resulting in a muscular tension. Accordingly, this tension causes the skin to deform and generates in superficial

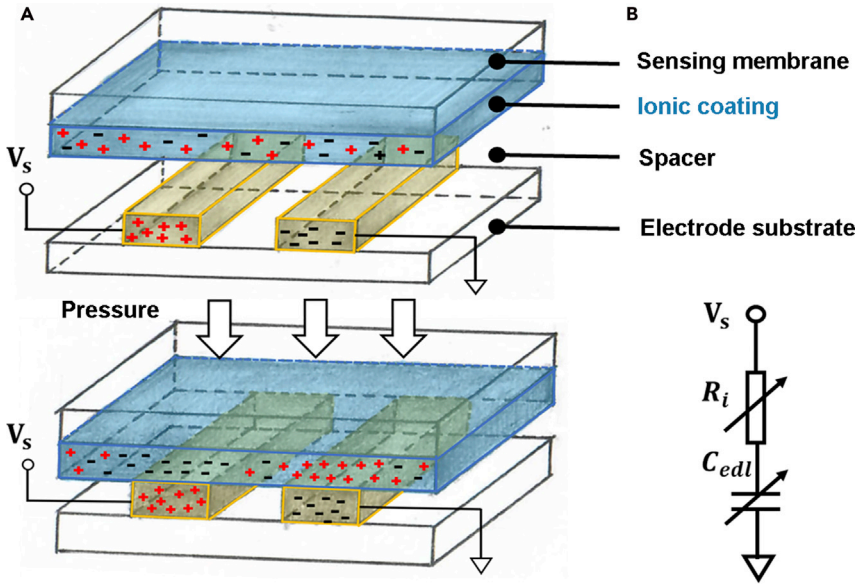

Figure 2. Iontronic sensing design

Illustration of the FITS sensing structure (A) along with its equivalent circuit diagram shown in (B).

pressure change (Zhang et al., 2019). Therefore, we have characterized this measurable variation in skin pressure and correlated it with muscular contraction through a manometry calibration. Furthermore, by embedding a highly sensitive yet structurally flexible iontronic sensor to the nose pad of the glasses, we can then continuously monitor the blink activities by tracking the muscular movements of orbicularis oculi muscles.

Iontronic sensing design

In order to detect the muscle-induced tension on the skin under the nose pad, the desired sensing system requires (1) high sensitivity; (2) small footprint; and (3) high signal-to-noise ratio (SNR), in addition to (4) its adaptiveness to the nose pad. Compared with the existing resistive and capacitive sensing technologies, the emerging flexible iontronic sensing (FITS) technology, invented by our team previously, offers the highest device sensitivity and the greatest SNR in a compact, flexible, and ultrathin packaging (Li et al., 2016, Li et al., 2017; Nie et al., 2012; Zhu et al., 2017). Superior performance of the FITS-enabled devices has been demonstrated in various similar yet challenging situations for detection of arterial pulsation and muscular activities. For example, an on-shoe monitoring system comprised of an FITS sensing array allows alignment-free capture of arterial pulse signals from the dorsalis pedis artery and matches the accuracy of the heart rate measurements within the clinical standard (Zhang et al., 2019). In addition, it can analyze the pedal postures by tracking the multiple tendon movements in real time. In this study, the FITS sensor has been incorporated into a standard glasses frame, specifically under the nose pad, given its flexible and thin packaging, which would not cause any discomfortable issue to the patients. More importantly, it can offer excellent device sensitivity with noise immunity to detect the skin pressure variations induced by the contraction of the orbicularis oculi muscles under a gentle pressure imposed by the glasses. Figure 2A illustrates the working principle of the FITS device. As can be seen, it consists of three functional layers: the top sensing membrane, which consists of the substrate and the ionic coating, and the layer with inter-digitated electrodes at the bottom, separated by a spacer in between with an air gap. Once the external pressure is applied toward the sensing membrane, it deforms and establishes a physical contact with the electrode, upon which the mobile ions and the free electrons in the respective layers would approach toward the interface within a nanometer separation, then inducing a substantial capacitive change. Accordingly, this interfacial capacitive value is in principle proportional to the area of the pressure-induced contact and can be detected electronically (Nie et al., 2012, 2015). A simplified equivalent circuit model has been included in Figure 2B, where C_{edl} stands for the pressure-induced interfacial capacitance upon contact, and R_i represents the internal resistance of the ionic coating. Detailed description of working principles and sensing structures can be found in the prior studies (Nie et al., 2012, 2015).

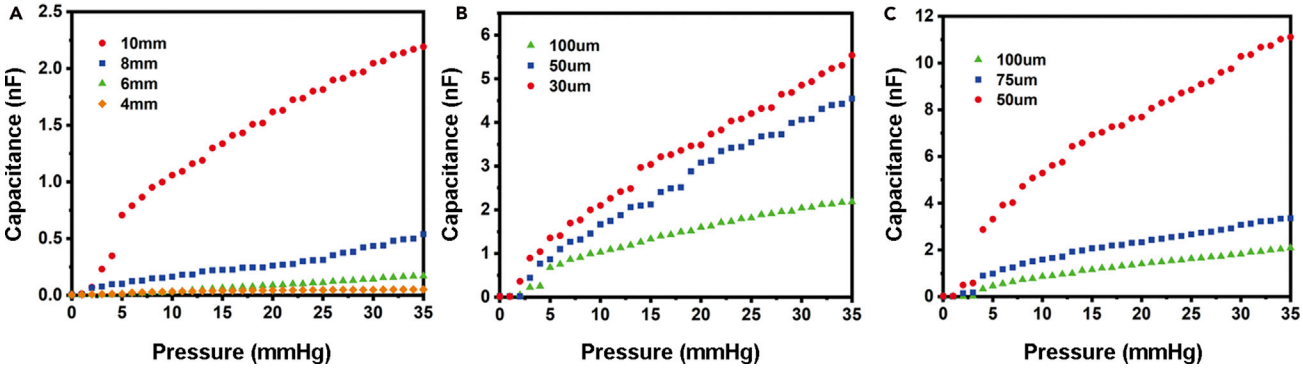

Figure 3. Characterization of the sensor performance

Characterization of the sensitivities of the FITS sensor under various geometric parameters. (A) Device sensitivities versus the diameters of the sensing chamber (4 mm, 6 mm, 8 mm, and 10 mm). (B) Device sensitivities versus the heights of the sensing chamber (100 μm, 50 μm, and 30 μm). (C) Device sensitivities versus the sensing membrane thicknesses (100 μm, 75 μm, and 50 μm).

Moreover, the sensing range has been targeted to be within 35 mmHg, because the hydrostatic pressure is typically considered to be less than 35 mmHg in the capillary bed, beyond which may compromise the microcirculation and perfusion, resulting in local hypoxia in skin in a continuous wear (Krogh et al., 1932). Therefore, such a design limit can serve as a physical boundary for a range of wearable devices in order to avoid hypoxia-induced uncomfortableness after extended usage.

RESULTS AND DISCUSSION

Characterization of the sensor performance

As aforementioned, the FITS sensors need to meet two design criteria, the first to provide high sensitivity in the range between 0 and 35 mmHg and the second to be fitted into the footprint of the nose pad. An optimization study between the sensor dimensions and sensitivities has been carried out, in which the sensors with various diameters and the heights of the sensing chamber as well as the thicknesses of the sensing membrane have been included.

In order to fit within the surface of the nose pad, we have limited the size of the sensing chamber to equal to or less than 10 mm in diameter under varying pressure loads. Consequently, four sensors with the sensing chamber sizes of 4, 6, 8, and 10 mm have been fabricated and tested, and the corresponding results have been summarized in Figure 3A, in which both the height and the thickness of the sensing membrane are fixed at 100 μm. It is worth noting that all these sensing membranes have the same thickness of the ionic coating, so that the sensitivity performance only relies on the deformability of the structural design (Zhang et al., 2019). From the classic membrane deformation theory, the diameter of sensing chamber has a significant influence on the device sensitivity (Nie et al., 2015), which is typically defined as the slope rate of the capacitive values versus the pressure changes. As exhibited in Figure 3A, the larger sensing chambers (of 8 mm and 10 mm in diameter) show significantly higher slope rates than those of the smaller chambers (of 4 mm and 6 mm in diameter). Specifically, the corresponding capacitances increase with the rise of pressure from 2 mmHg to 35 mmHg, which yields the device sensitivities measured at 1.6 pF/mmHg, 5.2 pF/mmHg, 16 pF/mmHg, and 66 pF/mmHg, respectively, for four different chamber sizes from the smallest to the largest ones. As a result, the devices with the larger chamber size exhibit higher device sensitivities. The sensor with the chamber diameter of 10 mm has the best performance in terms of the device sensitivity (i.e., 66 pF/mmHg) and therefore, is selected for further parametric studies.

Further optimization is to investigate the height of the sensing chamber. Accordingly, the sensors with different sensing chamber heights of 30 μm, 50 μm, and 100 μm have been fabricated and tested, similar to that of the size determination, given the chamber diameter of 10 mm and the sensing membrane thickness of 100 μm. As illustrated in Figure 3B, when the external pressure has been applied to the three sensor designs, it has yielded the device sensitivities of 66 pF/mmHg, 140 pF/mmHg, and 170 pF/mmHg, respectively, in the pressure range from 2 mmHg to 35 mmHg. Again, the lower chamber height results in a higher device sensitivity, which is consistent with the classic elastic deflection theory (Nie et al., 2015). Thus, the sensing chamber height is determined to be 30 μm.

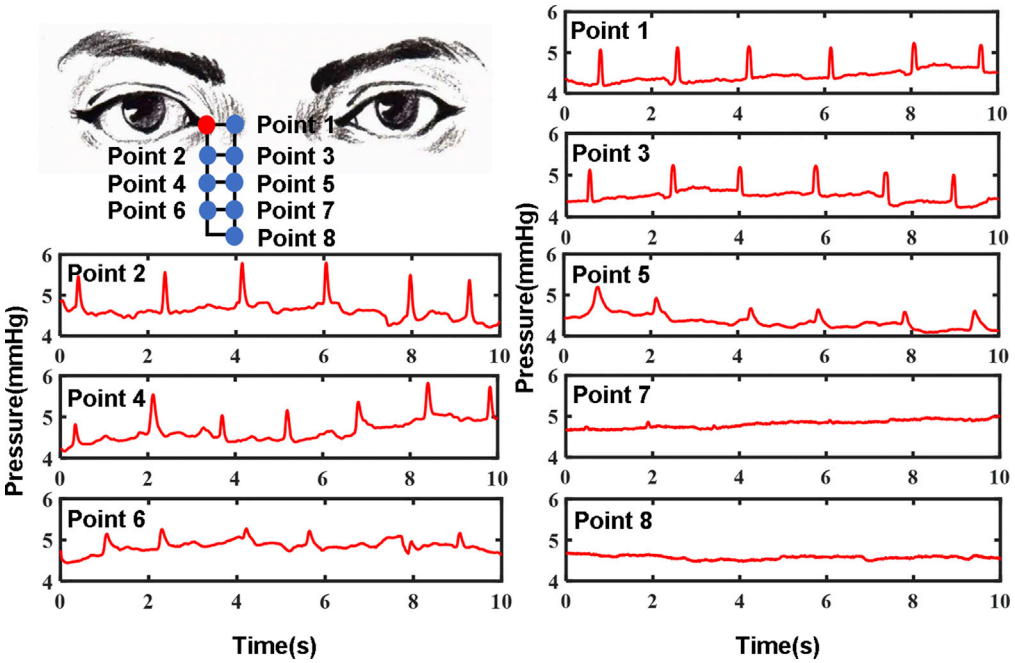

Figure 4. Optimization of the sensing location

Validation of the sensing locations within the blue grids, from which the corresponding signal waveforms have been measured (Note: the red dot indicates the inner canthus angle of eye as the anatomical reference).

Finally, the influence of the thicknesses of the sensing membrane has been investigated. The sensors with different thicknesses of the sensing membrane of 50 μm, 75 μm, and 100 μm are fabricated and tested, given the optimal sensing chamber diameter of 10 mm and the height of 30 μm. As shown in Figure 3C, the pressure-capacitance response curves have the similar trends as those measured in the first two graphs, which exhibit the sensitivities of 63 pF/mmHg, 100 pF/mmHg, and 340 pF/mmHg under the distinct thicknesses of the sensing membrane as aforementioned, within the same pressure range. This follows the trend that the thinner sensing membrane leads to a higher device sensitivity. As expected, the sensor with the thinnest sensing membrane of 50 μm has been chosen for the following blink-sensing study.

In summary, the desired sensor design has been determined from the comprehensive parametric studies, i.e., the one with the sensing chamber of 10 mm in diameter and 30 μm in height and the sensing membrane of 50 μm in thickness with the optimal sensitivity of 340 pF/mmHg. Given the electrode substrate of 100 μm in thickness, it has led to an overall device thickness of 180 μm and the effective area of 78.5 mm^2 in the FITS sensor, which can be amounted onto the nose pad seamlessly. Importantly, such a high-sensitivity design of the FITS sensor would ensure accurate and reliable detection of the skin pressure variations related to the muscular movements.

Optimization of the sensing location

In the consecutive study, we further investigate the optimal location around the nose pad for blink detection, by measuring the skin pressure variations during the muscular contraction. By using the inner canthus angle of the eye (as shown in Figures 1 and 4) as the anatomic reference of the coordinates, eight potential locations around the orbicularis oculi muscles are selected for measurements on an orthogonal grid with a side length of 5 mm, as illustrated in Figure 4, considering that the orbicularis oculi muscle around the lower eyelid is approximately 3–5 mm in width (Miller et al., 2010). It is worth noting that there are physiological limitations on selecting the measurement spots. For instance, it is difficult to place the sensor in a proximity to the canthus or on the bridge of the nose. The static load under the nose pad used in this study is measured around 4 mmHg by the FITS sensor, which is consistent with the published international standard for spectacle frames (BSI, 2004). Particularly, the FITS sensor is placed at the center of each measurement position with a static preload of 4 mmHg applied by a pneumatic bladder, whereas the variations of the skin pressure are recorded for a duration of one minute. Such a preload is stabilized by a pressure feedback

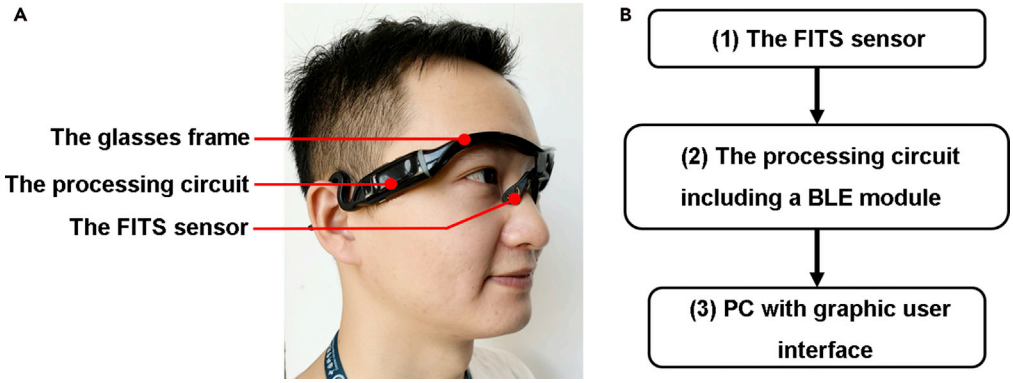

Figure 5. Blink-sensing glasses

(A) The blink-sensing glasses system on a health volunteer, along with (B) the illustration of its hardware building blocks.

provided from a connected clinical manometry (PicoPress) with an accuracy of less than 1 mmHg (Chi et al., 2017). The recorded data are summarized in Figure 4, from which blink patterns can be apparently extracted from the locations of P1-P4 with minimal interferences, whereas the blink patterns from P5 and P6 gradually attenuate in comparison. At the location of P7, it becomes relatively difficult to distinguish the blink pattern from the noises, whereas, the blink pattern is already indistinguishable at P8, possibly due to its furthest distance to the orbicularis oculi muscles anatomically. Specifically, the average amplitudes of blink patterns within one-minute duration are calculated at all eight locations as follows: 0.74 mmHg, 0.98 mmHg, 0.68 mmHg, 0.70 mmHg, 0.45 mmHg, 0.33 mmHg, 0.08 mmHg, and 0 mmHg from P1 to P8, respectively. These measurements suggest that the most effective area to detect the blink patterns is located within the area enclosed by P1-P4. On the other hand, the area covered by P1-P4 overlaps considerably with the area where the nose pad typically supports. As a conclusion, these results confirm the optimal location for detection of eye blink, which overlaps with that of the nose pad in a typical eyewear, using the relevant muscular movements.

Blink-sensing glasses

The blink-sensing glasses system has been devised and illustrated in Figure 5A, which is mainly composed of three parts: the FITS sensor, the processing circuit, and the glasses frame. The FITS sensor with high sensitivity is amounted onto the nose pad of glasses using adhesive and connected to the processing circuit via its flexible leads. A pair of commercial Bluetooth smart glasses (Gonbes K1) is adopted, which provides ample internal space for housing our electronic components and wire connections after the removal of its original acoustic components. The blink-sensing glasses is built to be reusable. The current prototype is weighted at 31.7g, of which the sensor and electronic parts is 5.6g. Specifically, as illustrated in Figure 5B, the pressure signals acquired from the FITS sensor (1) have been firstly processed by the processing circuit (2), in which the analog signal of pressure has been converted into the digital format, followed by wirelessly transmitting via the low-power Bluetooth module. The signal processing and statistical analysis have been conducted in a Bluetooth-enabled computer with graphic user interface developed (3). The main circuitry is controlled by a 32-bit microcontroller unit with an embedded ADC of 12-bit resolution (ST Microelectronics). The sampling rate of the data acquisition has been set at 125 Hz, which can be sufficient to catch the details in blink patterns, whereas the Bluetooth module transfers the pressure recordings at 1 Mbps wirelessly, enabling real-time data transmission. The overall current consumption of the system has been optimized at 2 mAh. With a battery capacity of 50 mAh, this blink-sensing wearable system can be theoretically extended more than 24 h continuously, supporting the continuous monitoring of full-day blinking activities for a patient.

To further illustrate the advantages of the proposed blink-sensing glasses over the counterpart devices published in recent years, Table 1 compares them side-by-side in terms of system size and complexity, data types, power consumptions, wearability, health hazard potential, environmental influence, and individual adaptability. Specifically, all the listed devices utilize noninvasive approaches to measure except the contact-lens means. Considering the system size and wearability, the contact lens and infrared sensors along with our blinking-sensing glasses have the smallest footprints and could be worn in a continuous

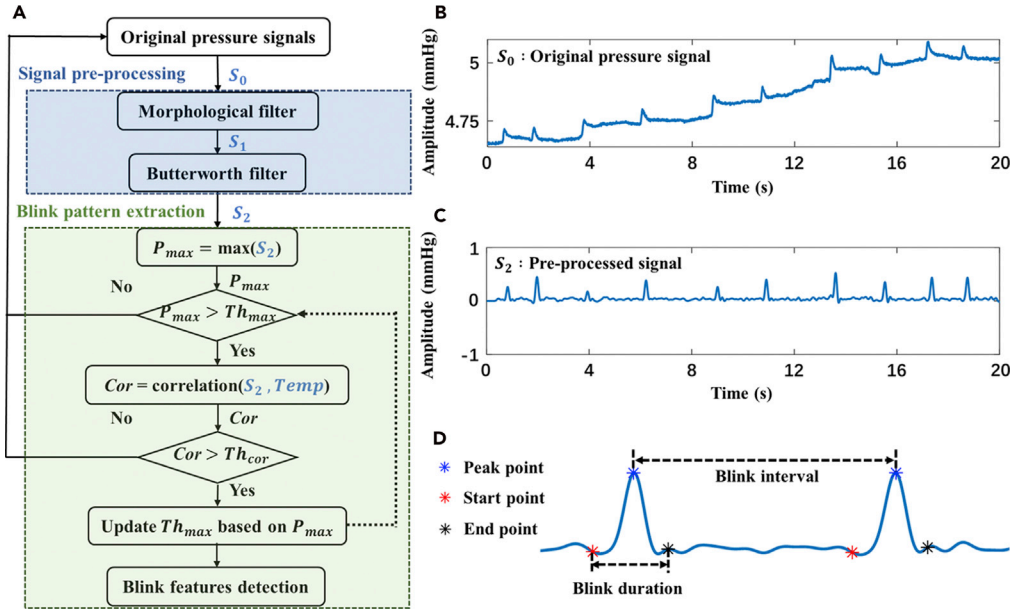

Figure 6. Blink-detection algorithm 1

(A) Flowchart of the blink-detection algorithm, and plots of (B) the original pressure waveform of S_0, which contains multiple blink activities with a 20-s window, (C) the pre-processed signals of S_2 following the morphological and Butterworth filters, with (D) the detected blink features, i.e., the peak, the start, and the endpoints, using the template matching method.

manner (Dementyev and Holz, 2017). However, the contact lens and infrared sensors may still pose potential health hazard to the eye (Wolbarsht, 1980; Faschinger and Mossbck, 2010). Also, all the optical-based methods are highly subject to ambient light conditions, which might introduce additional environmental noises to the results (Taner et al., 2010; Fogelton and Benesova, 2018). Moreover, the facial structure varied on individuals might have additional side effects on the optical-based approaches, which needs additional algorithms to compensate (Dementyev and Holz, 2017). However, the proposed blink-sensing glasses may experience reliability issues under the severe motion artifacts caused by extreme facial expressions or the poor contact with the skin when improperly worn. For the adaptability consideration, the infrared sensor typically needs to be amounted onto two locations on the glasses, i.e., the emitting unit on one side with the receiving unit on the other side of the lens, and therefore, it is highly vulnerable to the facial influence of the subject, whereas the pressure-based measurement only relies on the single-point contact between the nose pad and the skin. Therefore, the sensor needs to be placed in a reliable contact with the skin for continuous measurements. To further improve the reliability of our approach, the future iteration of the blink-sensing glasses can include one pressure sensor on each pad. In addition, the use of the blink-sensing glasses is currently limited to indoor testing where the temperature and humidity are highly controlled and the subjects are under a quiescent condition. In conclusion, the blink-sensing glasses offer combined advantages of its compact footprint, long-term wearability, safety, and immunity to environmental and individual influences, in addition to its low power consumption, over the existing technologies.

Blink-detection algorithm

Comparing it with the standard video recordings, the signals of skin pressure variations (S_0) collected by the blink-sensing glasses contain the following characteristics. First of all, the raw signals have appreciable pressure variations during the corresponding blink events, which can be potentially used to compute the blink features. Secondly, there are present severe baseline drifts, possibly induced by the motion, along with high-frequency noises from the hardware and ambient electromagnetics (Xia et al., 2012). Therefore, we have implemented a two-stage blink-detection algorithm by firstly applying a classic pre-processing step to remove the undesired noises and drifts, and secondly subsequently extracting the blink-patterns using a template-matching approach, as illustrated in Figure 6A. Specifically, a morphological filter and a Butterworth filter are used in sequence for the signal pre-processing. As a nonlinear filter without considering noise frequency, the morphological filter is highly suitable to remove baseline drifts with uncertainty

by employing a series of opening, dilation, closing, erosion operations in sequence (Loce, 1992). By subtracting it from the original pressure signal S_0 in Figure 6B, the baseline drift is removed afterward to obtain the stable signal of S_1. Then, the subsequent Butterworth low-pass filter is implemented to remove high-frequency noises. It is designed as an eighth-order filter with a cut-off frequency of 5 Hz, which can effectively filter out the blink signals from the EOG and other electromagnetic noises from the hardware and environment (Yi et al., 2010). As a result, the pre-processed signal of S_2, as shown in Figure 6C, exhibits as a smooth curve with a flat baseline and is readily available for blink pattern extraction.

For the blink-pattern extraction, the template matching method has been applied, because it is widely used in detecting patterns in quasi-periodic biomedical signals (Chin et al., 2010; Kim and Mcnames, 2007). For example, different templates have been used to detect ECG waveforms, from which the accuracy of the detection in some characteristic bands could reach up to 100%, according to Chin's study (Chin et al., 2010). Specifically, an initial template needs to be prepared in advance. In this case, the blink data have been collected in a 10-min window from 12 volunteers, using both the pressure and video means simultaneously. The blink data are then marked according to the video standard and averaged into the pre-generated template, marked as *Temp* in Figure 6A, of which the minimum peak value is denoted as Th_0. In the consecutive step, the pre-processed signals with blink patterns are applied to matching the specific amplitude and shape criteria with two threshold values of Th_{max} and Th_{cor} correspondingly. Particularly, the amplitude matching criteria of Th_{max} is not set as a fixed value, because the pressure amplitude of the blink patterns may vary from time to time. To tackle such a challenge, a template processing approach has been proposed in a prior art (Kim and Mcnames, 2007), where the threshold of amplitude can be dynamically adjusted in a linear expression, based on the features of the signals calculated from the previous period. Specifically, the threshold value is defined as $Th_{max} = Th_0 + v^*(P_0 - Th_0)$, where Th_0 is the minimal amplitude of the blink patterns in the initial recordings, whereas P_0 is extracted as the average peak value (P_{max}) from the previous blink patterns. In addition, v stands for a user-specified parameter to ensure that the magnitude of the noise is always lower than that of the effective signal (Kim and Mcnames, 2007), which greatly reduces the false detection. In this case, v is determined to be 0.1 based on the estimation of the average magnitude ratio of noises and blink patterns in the pre-processed signal. This formula ensures that the threshold Th_{max} is greater than the amplitude of noise to the greatest extent. When the peak value of the pre-processed signal P_{max}, representing the amplitude of the waveform, is greater than that of Th_{max}, it is considered to meet the amplitude criteria. On the other hand, a correlation coefficient could be calculated to measure the shape similarity between the detected signals and the pre-generated template. Combined our evaluation results with previous reference (Chin et al., 2010), the threshold of Th_{cor} has been fixed to 0.98. Only when both criteria are satisfied, it is considered as a blink pattern.

Figure 6D shows the detected blink patterns with the peak points labeled using the template matching method. After locating the peak points of blink patterns, the next step is to determine the start and endpoints of the blink patterns, which are simply defined as the extreme points prior to and after the peak value. Once the blink patterns with three key feature points (i.e., peak, start point, and endpoint) have been identified, the critical blink features can be then computed according to the literatures (Hamrah and Foulks, 2005; Inomata et al., 2018), i.e., blink rate (i.e., the number of peaks in a minute), blink interval (i.e., the time difference between two consecutive peaks), and the blink duration (i.e., the time difference between the start and the endpoints), as illustrated in Figure 6D. These blink features are of critical importance to distinguish the dry-eye patients (Hamrah and Foulks, 2005; Rodriguez et al., 2013).

To evaluate the performance of the blink-detection algorithm, the blink pattern extraction results derived from the pressure variations are compared with that of the conventional video approach, which is considered as the clinical standard currently (Rodriguez et al., 2013; Jürgen et al., 2017; Taner et al., 2010; Fogelton and Benesova, 2018). According to the literature, the conventional video approach employs manual operations to mark the blink patterns from the recordings (Rodriguez et al., 2013; Wang et al., 2018; Kazuo, 1998), from which we have adopted the same procedure as the standard to this study. The date sets used to verify the accuracy of the algorithm are collected from four volunteers when they are working on computers. Two and a half hours of data are collected, as described in method section. Figure 7A plots typical synchronous waveforms with blink patterns recorded by both the pressure-sensing and video means during a 10-s period. As described previously, the pressure variations (colored in blue) are processed in a normalized scale with the removal of the baseline drift, whereas the height of the eye aperture (colored in red) has been calculated and normalized from each frame of the video recording as a reference. The height of

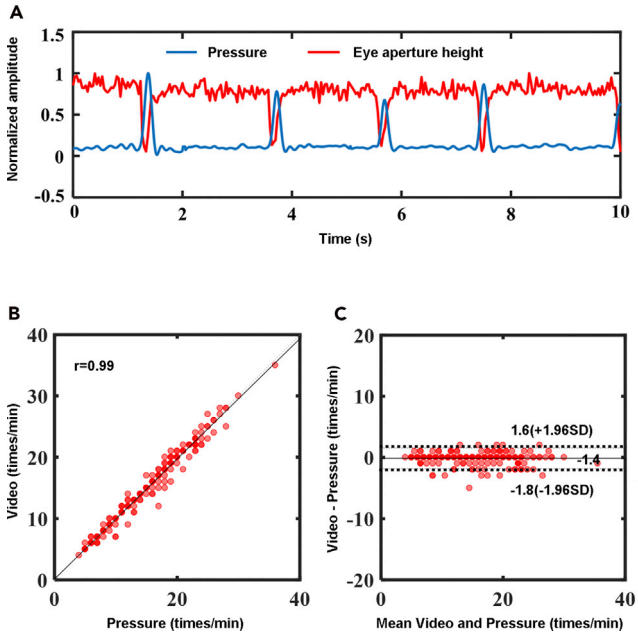

Figure 7. Blink-detection algorithm 2

(A) Eye aperture height change curve (red) and pressure change curve (blue) normalized at the same scale.

(B) Correlation between the blink rate calculated by pressure signal and the blink rate calculated by video.

(C) Bland Altman plot of blink rate that the blink-sensing glasses extract and that from the video. The horizontal and vertical axes are the mean and difference values of blink rates that the blink-sensing glasses measure and that from the video, respectively.

the eye aperture is calculated according to the literature (Houssaini et al., 2019). As expected, these two signal streams are highly synchronized with matching peak/valley patterns to indicate the blink patterns. Figure 7B compares the analytical results of the blink rates from these two methods in the 2.5-h continuous recording, consistently exhibiting highly correlated outcomes with a correlation coefficient of 0.99. Moreover, the Bland-Altman plot is frequently utilized as a statistic tool to compare the new method with the existing gold standard (Myles and Cui, 2007). As shown in Figure 7C, it exhibits a low mean error of −0.14 blinks/min between the video results and the pressure measurements, which means that the systematic errors between the two methods fall into a small margin. The black dashed lines represent a 95% confidence interval and ranges from −1.8 to 1.6 blinks/min, and more than 95% (142/150) of the points are within the confidence interval, illustrating no obvious deviation between the results detected by the proposed system (pressure-sensing) and the gold standard (video).

In addition to the accuracy of Bland Altman plot description, the confusion matrix that can describe the accuracy more specifically has also been carried out on the same datasets. Table 2 summarizes the statistical findings, in which 2,776 blink patterns have been marked in the video, whereas 2,774 blink patterns can be detected by the blink-sensing glasses. An overall accuracy of 96.3% has been achieved with 53 blink patterns missed and 51 ones falsely counted. The false positives can possibly attribute to the weak signals of blink patterns overwhelmed by the noises from motion artifacts, whereas the false negatives may be caused by the poor physical contact between the sensor and the skin of the testing objects. Together, these results have confirmed that both high statistic consistency and high accuracy have been presented in the sensing results between the new blink-detecting method and the video-based gold standard, which has reportedly reached an accuracy of 97.6% in the clinical literatures (Kazuo, 1998; Fogelton and Benesova, 2018). In summary, the detection results of the blink-sensing glasses can satisfy the accuracy requirement of clinical blinking analysis, while providing a convenient and continuous wearable means to monitor the blink activities in a minimally interruptive manner.

A demonstration of dry-eye analysis

To demonstrate the clinical utilities of the blink-sensing glasses, we comparatively analyses the differences in the blink patterns between healthy subjects and dry-eye patients. Dry-eye analysis has been selected

Table 2. The confusion matrix of detection algorithm

		The number of blink patterns in the video	
		Positive	Negative
The number of blink patterns extracted by algorithm	Positive	(TP)2723	(FP)51
	Negative	(FN)53	(TN)0

because the blink patterns and the dry-eye symptoms are closely related, from which significant time-domain differences in blink features, i.e., the blink rate, interval, and duration, have been reportedly found between the dry-eye patients and healthy subjects, as aforementioned. Specifically, one of the major causes for the dry-eye disease is the tear film instability occurred on the ocular surface (Wang et al., 2018). To maintain the tear film of the dry-eye patients, it would require a higher blink rate than that of healthy subjects (Tsubota et al., 1996). Similarly, a shorter blink interval would result from the faster blink rate (Tsubota et al., 1996; Hamrah and Foulks, 2005). Furthermore, several studies have shown that a longer blink duration is expected to alleviate ocular discomfort in those patients (Rodriguez et al., 2013).

One-hour blink data from six subjects have been collected by the blink-sensing glasses, of which three are dry-eye patients and healthy subjects classified by the clinical OSDI scores (Wang et al., 2018; Kazuo, 1998; Tsubota et al., 1996; Hamrah and Foulks, 2005; Rodriguez et al., 2013). The average score of OSDI scale of the dry-eye subjects is 32.7 ($\pm$7.5), whereas that of the healthy subjects is 11.3 ($\pm$1.1). The blink features from two groups are compared statistically using the one-way analysis of variance (ANOVA), which is typically used to determine whether there are any statistically significant differences between the means of groups for blinking analysis (Kazuo, 1998; Tsubota et al., 1996; Hamrah and Foulks, 2005; Rodriguez et al., 2013).

The results have been summarized in Figure 8. As expected, the average blink rate from the dry-eye subjects is 20.5 ($\pm$4.0) times/min, as compared with that of the healthy subjects (i.e., 15.6 ($\pm$3.0) times/min). According to the one-way ANOVA, the blink rate of the dry-eye subjects is significantly higher than that of the healthy subjects ($P = 0.001$). This conclusion is consistent with several prior studies (Wang et al., 2018; Kazuo, 1998; Tsubota et al., 1996; Hamrah and Foulks, 2005). Similarly, the blink duration of the patients is averaged at 0.69 ($\pm$0.13) sec, which is also higher than that of the healthy subjects (of 0.60 ($\pm$0.12) sec), and a significant difference ($P = 0.013$) presents in the blink duration between the two groups using the one-way ANOVA, which is also consistent with the previous results (Tsubota et al., 1996; Hamrah and Foulks, 2005). Finally, the maximum blink intervals have been calculated as 8.07 ($\pm$2.74) sec for the dry-eye patients and 9.45 ($\pm$2.36) sec for the healthy controls, respectively. The feature measured from the patients is also statistically substantially lower than that of the healthy subjects ($P = 0.041$), which again well matches with that of the prior studies (Hamrah and Foulks, 2005; Rodriguez et al., 2013). As a conclusion, the blink-sensing glasses could be of potential clinical use to diagnose as well as to prognose the dry-eye symptoms in a continuous and wearable manner.

Conclusion

In this paper, a novel blink-sensing glasses embedding the FITS sensor with high sensitivity has been successfully implemented to monitor the movement of the orbicularis oculi muscles and achieve continuous eye-blink monitoring. In particular, the blink-sensing glasses offer highly accurate (96.3%) and long-term continuous monitoring of eye blink process in a truly comfortable and wearable fashion. Specifically, we have experimentally identified the nose pad as a desirable location to track the muscular movements related to eye blinks. Accordingly, the FITS sensor with the sensitivity of 340 pF/mmHg is integrated onto the nose pad, whereas the rest of the system is hosted within the glasses frame, from which the recorded data can be transmitted to a wireless terminal. By applying the template-matching algorithm with variable thresholds, the detection results have been compared with the clinical standards using Bland-Altman plot and confusion matrix, from which high statistic consistency and high accuracy can be confirmed. As the final demonstration, the differences in the blink patterns between healthy volunteers and dry-eye patients have been comparatively analyzed. Consistent with the findings from the previous studies, statistical differences have been observed in the features of blink patterns, i.e., the blink rate, maximum blink interval, and blink duration, between the patients and the control group. And therefore,

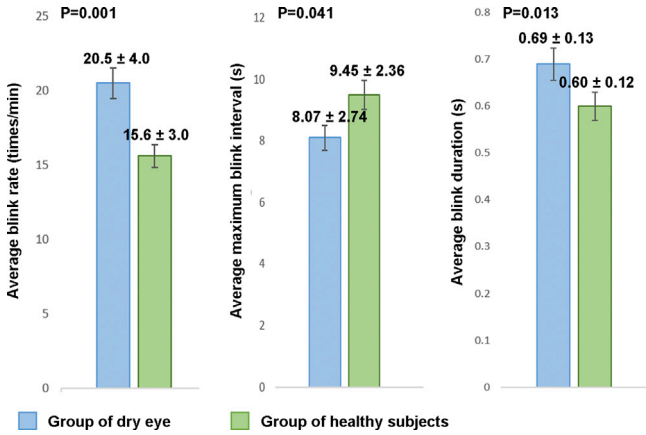

Figure 8. A demonstration of dry-eye analysis. Statistical chart of blink features including average blink rate, average maximum blink interval, and average blink duration, comparing between dye-eye patients and healthy subjects.

the blink-sensing glasses wearable within the high level of accuracy can be potentially used as an alternative clinical-grade monitoring tool for eye blink analysis, while providing patients with high comfortableness of long-term ambulatory and home use.

Limitations of the study

As aforementioned in "Blink-sensing glasses" of Results and Discussion, the pressure-based measurement only relies on the single-point contact between the nose pad and the skin. Therefore, the sensor needs to be placed in a reliable contact with the skin for continuous measurements. In addition, the use of the blink-sensing glasses is currently limited to indoor testing where the temperature and humidity are highly controlled and the subjects are under a quiescent condition.

Resource availability

Lead contact

Further information and requests for resources and reagents should be directed to and will be fulfilled by the lead contact, Tingrui Pan (tingrui@ucdavis.edu).

Materials availability

This study did not generate new unique reagents.

Data and code availability

The datasets supporting the current study have not been deposited in a public repository but are available from the corresponding author on request.

METHODS

All methods can be found in the accompanying transparent methods supplemental file.

SUPPLEMENTAL INFORMATION

Supplemental information can be found online at https://doi.org/10.1016/j.isci.2021.102399.

ACKNOWLEDGMENTS

This research was in part supported by Shenzhen fundamental research program (Grant No. JCYJ20170413164102261), Guangdong program (Grant No. 2016ZT06D631), National Natural Science Foundation of China (Grant No. 61903355), and Shenzhen engineering laboratory of single-molecule detection and instrument development (Grant No. XMHT20190204002). The authors would like to thank Dr. Yu Chang for his advice on FITS sensor design and characterization. The authors would acknowledge *TacSense*, Inc. for providing the sensor manufacturing service.

AUTHOR CONTRIBUTIONS

Conceptualization, T.P. and D.W.; Methodology, R.C., Z.Z., H.K., L.C., and K.D.; Software, R.C.; Validation, R.C., K.D., and Z.Z.; Formal Analysis, R.C.; Investigation, R.C.; Resources, T.P. and K.D.; Writing—Original Draft, R.C., Z.Z., and K.D.; Writing—Review & Editing, T.P.; Visualization, R.C.; Supervision, T.P.; Funding Acquisition, T.P. and K.D.

DECLARATION OF INTERESTS

The authors declare no competing interests.

Received: December 25, 2020
Revised: March 15, 2021
Accepted: April 2, 2021
Published: May 21, 2021

REFERENCES

Anat, G., Naresh, K., William, F., and David, J.L. (2014). Environmental factors affect the risk of dry eye syndrome in a United States veteran population. Ophthalmology *121*, 972–973.

Aristea, L., Christos, F., Panagiotis, B., and Ana, B.V. (2014). Eye blink rate as a biological marker of mild cognitive impairment. Int. J. Psychophysiology *93*, 12–16.

Bryant, J.J., and Lorenza, S.C. (2016). Spontaneous eye blink rate as predictor of dopamine-related cognitive function—a review. Neuroence Biobehavioral Rev. *71*, 58–82.

BSI (2004). BS EN ISO 12870: 2004 Spectacle Frames. General Requirements and Test Methods (British Standards Institute).

Chambayil, B., Singla, R., and Jha, R. (2010). EEG eye blink classification using neural network. Lecture Notes Eng. Comput. Sci. *2183*.

Chi, Y.W., Tseng, K.H., Li, R., and Pan, T. (2017). Comparison of piezoresistive sensor to PicoPress in in-vitro interface pressure measurement. Phlebology *33*, 315–320.

Chin, F.J., Fang, Q., Zhang, T., and Cosic, I. (2010). A fast critical arrhythmic ECG waveform identification method using cross-correlation and multiple template matching. Annu. Int. Conf. IEEE Eng. Med. Biol. Soc. *2010*, 1922–1925.

Dementyev, A., and Holz, C. (2017). DualBlink: a wearable device to continuously detect, track, and actuate blinking for alleviating dry eyes and computer vision syndrome. Proc. ACM Interact. Mob. Wearable Ubiquitous Technol. *1*, 1–19, https://doi.org/10.1145/3053330.

Faschinger, C., and Mossbck, G. (2010). Continuous 24 h monitoring of changes in intraocular pressure with the wireless contact lens sensor triggerfish. first results in patients. Ophthalmologe *107*, 918–922.

Fogelton, A., and Benesova, W. (2018). Eye Blink Completeness Detection (Computer Vision and Image Understanding), pp. 176–177.

Frigerio, A., Hadlock, T.A., Murray, E.H., and Heaton, J.T. (2014). Infrared-based blink-detecting glasses for facial pacing: toward a bionic blink. Jama Facial Plast. Surg. *16*, 211–218.

Geyer, M., and Braff, D. (2010). Habituation of the blink reflex in normals and schizophrenic patients. Psychophysiology *19*, 1–6.

Hamrah, P., and Foulks, G.N. (2005). Characteristics of optical aberrations in dry eye patients with increasing blink intervals. Ocul. Surf. *3*, S72.

Xia, H., Garcia, G.A., Mcbride, J.C., Sullivan, A., and Zhao, X. (2012). Computer algorithms for evaluating the quality of ECGs in real time. 2011 Computing in Cardiology (IEEE).

Houssaini, A.S., Sabri, M.A., Qj Idaa, H., and Aarab, A. (2019). Real-Time Driver's Hypovigilance Detection using Facial Landmarks. 2019 International Conference on Wireless Technologies, Embedded and Intelligent Systems (WITS) (IEEE).

Inomata, T., Okumura, Y., Fujimoto, K., and Shiang, T. (2018). Maximum blink interval is associated with tear film breakup time: a new simple, screening test for dry eye disease. Sci. Rep. *8*, 13443.

Jacobsen, L. (1996). Blink rate in childhood-onset schizophrenia: comparison with normal and attention-deficit hyperactivity disorder controls. Biol. Psychiatry *40*, 1222–1229.

Jürgen, S., Laarousi, R., Stolzmann, W., and Katja, K. (2017). Eye blink detection for different driver states in conditionally automated driving and manual driving using EOG and a driver camera. Behav. Res. Methods *50*, 1–14.

Karson, C.N., Burns, R.S., LeWitt, P.A., Foster, N.L., and Newman, R.P. (1984). Blink rates and disorders of movement. Neurology *34*, 677–678.

Katsarava, Z., Giffin, N., Diener, H.C., and Kaube, H. (2010). Abnormal habituation of 'nociceptive' blink reflex in migraine–evidence for increased excitability of trigeminal nociception. Cephalalgia *23*, 814–819.

Kazuo, T. (1998). Tear dynamics and dry eye. Prog. Retin. Eye Res. *17*, 565.

Kim, S., and Mcnames, J. (2007). Automatic spike detection based on adaptive template matching for extracellular neural recordings. J. Neurosci. Methods *165*, 165–174.

Korb, D.R., Grenon, S.M., Blackie, C., Willis, T.R., and Bacich, S. (2017). Apparatuses and Methods for Determining Tear Film Break-Up Time And/or for Detecting Lid Margin Contact and Blink Rates, Particularly for Diagnosing, Measuring, And/or Analyzing Dry Eye Conditions and Symptoms (WO).

Krogh, A., Landis, E.M., and Turner, A.H. (1932). The movement of fluid through the human capillary wall in relation to venous pressure and the colloid osmotic pressure of the blood. Clin. Invest. *11*, 63–95.

Lai, R. (2001). Book reviews: electrodiagnosis in diseases of nerve and muscle: principles and practice 3rd edn edited by jun kimura. Eur. J. Paediatr. Neurol. *5*, 269–270.

Li, M., Gong, L., Chapin, W.J., and Zhu, M. (2012). Assessment of vision-related quality of life in dry eye patients. Invest. Ophthalmol. Vis. Sci. *53*, 5722–5727.

Li, R., Nie, B., Zhai, C., Cao, J., Pan, J., Chi, Y.W., and Pan, T. (2016). Telemedical wearable sensing platform for management of chronic venous disorder. Ann. Biomed. Eng. *44*, 2282–2291.

Li, R., Si, Y., Zhu, Z., Guo, Y., Zhang, Y., Pan, N., Sun, G., and Pan, T. (2017). Super capacitive iontronic nanofabric sensing. Adv. Mater. *29*, 1700253.

Lin, P.-H., Chang, W.-L., Sheu, S.-C., and Li, B.-R. (2020). A noninvasive wearable device for real-time monitoring of secretion sweat pressure by digital display. iScience *23*, 101658.

Loce, R.P. (1992). Facilitation of optimal binary morphological filter design via structuring element libraries and design constraints. Opt. Eng. *31*, 1008–1025.

Miller, F.P., Vandome, A.F., and Mcbrewster, J. (2010). Orbicularis Oculi (Muscle Alphascript Publishing).

Mller, A.R. (1991). Interaction between the blink reflex and the abnormal muscle response in patients with hemifacial spasm: results of intraoperative recordings. J. Neurol. Sci. *101*, 114–123.

Myles, P.S., and Cui, J. (2007). Using the bland-altman method to measure agreement with repeated measures. Br. J. Anaesth. *99*, 309–311.

Nie, B., Siyuan, X., James, D.B., and Tingrui, P. (2012). Droplet-based interfacial capacitive sensing. Lab Chip *12*, 1110–1118.

Nie, B., Li, R., Cao, J., Brandt, J.D., and Pan, T. (2015). Flexible transparent iontronic film for interfacial capacitive pressure sensing. Adv. Mater. *27*, 6055–6062.

Pan, T., and Xu, Y. (2014). Mobile medicine: can emerging mobile technologies enable patient-oriented medicine? Ann. Biomed. Eng. *42*, 2203–2204.

Rodriguez, J.D., Lane, K.J., Ousler, G.W., Angjeli, E., and Abelson, M.B. (2016). Diurnal tracking of blink and relationship to signs and symptoms of dry eye. Cornea *35*, 1104–1111.

Rodriguez, J.D., Ousler, G.W., 3rd, Johnston, P.R., Lane, K., and Abelson, M.B. (2013). Investigation of extended blinks and interblink intervals in subjects with and without dry eye. Clin. Ophthalmol. *7*, 337–342.

Shahani, B. (1970). The human blink reflex. J. Neurol. Neurosurg. Psychiatry *33*, 792–800.

Silverstein, L., and Graham, F. (2010). Eyeblink EMG: a miniature eyelid electrode for recording from orbicularis oculi. Psychophysiology *15*, 377–379.

Stern, J.A., Boyer, D., and Schroeder, D. (1994). Blink rate: a possible measure of fatigue. Hum. Factors *36*, 285–297.

Taner, D., Ian, M.B., Chabane, D., and Nacim, I. (2010). Drowsy Driver Detection System Using Eye Blink Patterns, International Conference on Machine & Web Intelligence (*IEEE*).

Tsikriteas, Z.M., Roscow, J.I., Bowen, C.R., and Khanbareh, H. (2020). Flexible ferroelectric wearable devices for medical applications. iScience *24*, 101987.

Tsubota, K., Hata, S., Okusawa, Y., Egami, F., Ohtsuki, T., and Nakamori, K. (1996). Quantitative videographic analysis of blinking in normal subjects and patients with dry eye. Arch. Ophthalmol. *114*, 715–720.

Vermeulen, N., Godefroid, J., and Mermillod, M. (2009). Emotional modulation of attention: fear increases but disgust reduces the attentional blink. PLoS One *4*, e7924.

Wang, M.T.M., Tien, L., Han, A., Lee, J.M., Kim, D., Markoulli, M., and Craig, J.P. (2018). Impact of blinking on ocular surface and tear film parameters. Ocul. Surf. *16*, 424–429.

Wang, L., Xu, T., Fan, C., and Zhang, X. (2020). Wearable strain sensor for real-time sweat volume monitoring. iScience *24*, 102028.

Wolbarsht, M. (1980). Damage to the lens from infrared. Proc. SPIE *229*, 121–143.

Wu, S.L., Liao, L.D., Lu, S.W., Jiang, W.L., and Lin, C.T. (2013). Controlling a human-computer interface system with a novel classification method that uses electrooculography signals. IEEE Trans. Biomed. Eng. *60*, 2133–2141.

Yi, J., Su, F., & Cai, A., (2010). A hybrid RABWC-STF method for eye-blink removal from EEG. Proceedings of the IEEE International Conference on Systems, Man and Cybernetics, Istanbul, Turkey, 10-13 October 2010. IEEE.

Yi, X., Jia, J., Deng, S., Shen, S.G., Xie, Q., and Wang, G. (2013). A blink restoration system with contralateral emg triggered stimulation and real-time artifact blanking. IEEE Trans. Biomed. Circuits Syst. *7*, 140–148.

Zhang, Z., Zhu, Z., Bazor, B., Lee, S., Ding, Z., and Pan, T. (2019). Feetbeat: a flexible iontronic sensing wearable detects pedal pulses and muscular activities. IEEE Trans. Biomed. Eng. *66*, 3072–3079.

Zhu, Z., Li, R., and Pan, T. (2017). Imperceptible epidermal–iontronic interface for wearable sensing. Adv. Mater. *30*, 1705122.1–1705122.9.

iScience, Volume *24*

Supplemental information

Blink-sensing glasses: A flexible iontronic sensing wearable for continuous blink monitoring

Rui Chen, Zhichao Zhang, Ka Deng, Dahu Wang, Hongmin Ke, Li Cai, Chi-wei Chang, and Tingrui Pan

Supplemental Information

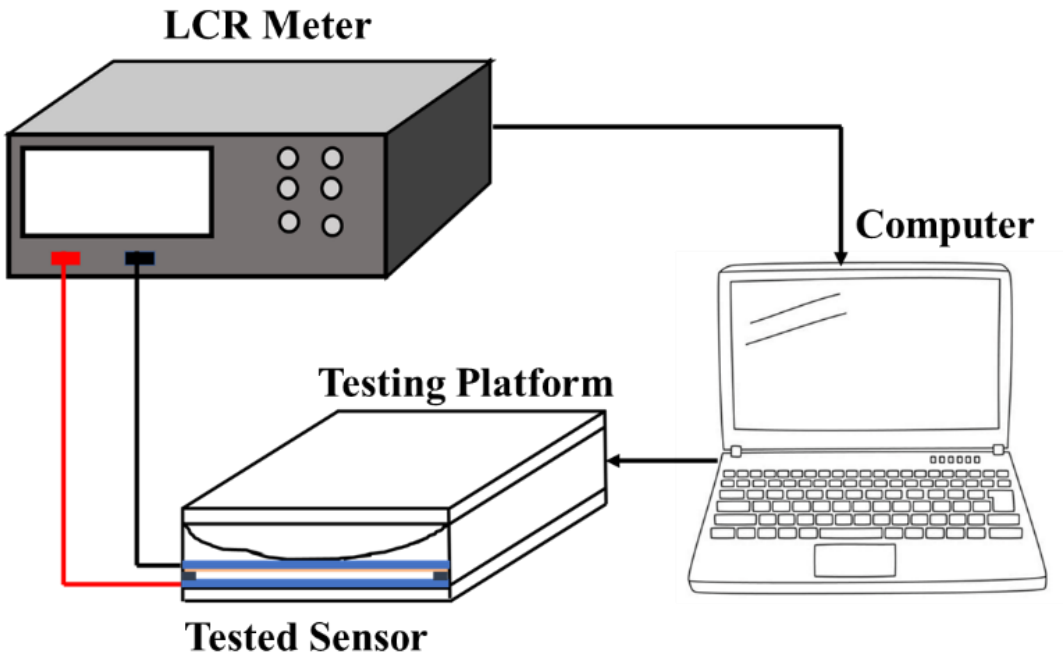

Fig. S1 The structure diagram of the test platform. Related to Fig. 3 and Fig. 4.

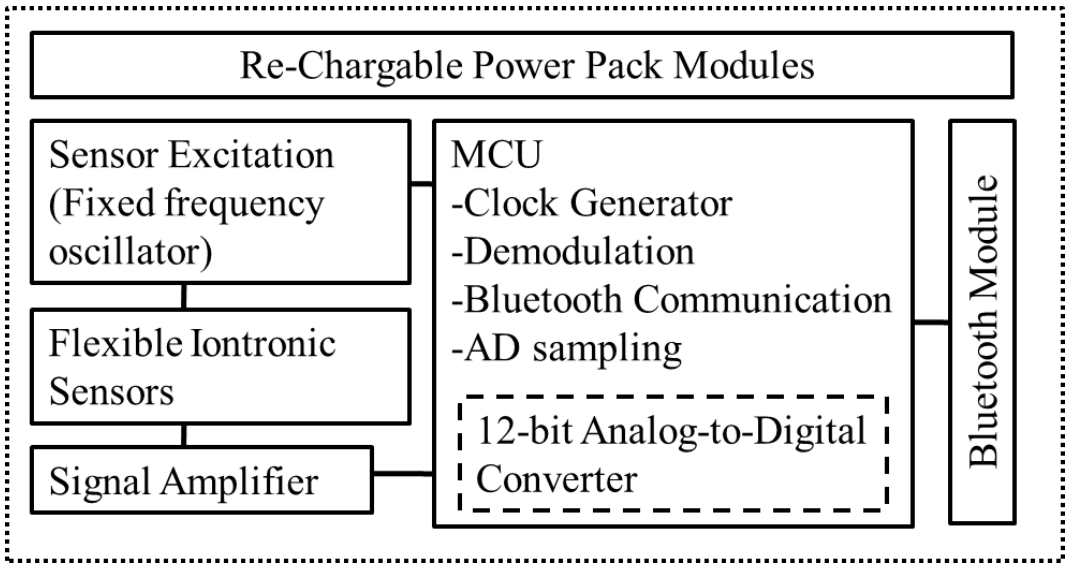

Fig. S2 The circuit diagram of Blink-sensing glasses. Related to Fig. 5.

Fig.S3 The photo of blink-sensing glasses. Related to Fig. 5.

Table S1 The cost estimation of blink-sensing glasses. Related to Table 1.

Components	Price
The FITS sensor	10 USD
The glasses frame	~ 10 USD
Circuit board	~ 20 USD

Table S2 The subject details of dry eye test. Related to Fig. 8.

	Age	Gender	OSDI scale
Healthy subject 1	31	Man	12.50
Healthy subject 2	26	Man	11.00
Healthy subject 3	25	Female	10.25
Dry eye subject 1	24	Female	25.00
Dry eye subject 2	27	Female	40.00
Dry eye subject 3	24	Female	33.00

Transparent Methods

A. Sensor Calibration Platform

In order to test the sensor performance, a customized testing platform was used. It was able to generate uniform pressure loading within ±1 mmHg accuracy in the range of 0-300mmHg by a delicate pneumatic control system. The test platform structure was shown in Fig. S1. When the system started working, a certain pressure was applied to the sensor. The output of the tested sensor was read out by an LCR meter (E4980AL, *Keysight*) in the form of capacitance. The variation of the capacitance was recorded in real-time and matched with the controlled pressure generated by the system on the computer. The test platform was calibrated by a dynamometer (GM520, *Benetech*®) to ensure the accuracy of the pressure generated by the system.

Through the test, the response curve between the pressure and the capacitance values was obtained, from which the sensitivity of the sensor was calculated (Fig. 3). This pressure-capacitance curve (Fig. 4) was used to convert the response of the sensor into the pressure levels during blinks in the following studies. In the surface performance test, the sensor was pasted on the surface with different radius to test the sensitivity. In the temperature stability test, the sensor was placed at 10-50 ℃, and the capacitance per unit area was measured (VICTOR 4080) at different temperatures.

B. Skin pressure characteristics

The pressure variation was measured at eight positions near the inner canthus angle to find the appropriate location to capture skin pressure response during blinks. At each point, the sensor with the optimized dimensions which satisfied the a forementioned measurement range of 0-35 mmHg was pressed at the target location by a manometry (PicoPress™) with a static pressure of 4 mmHg based on the estimation of the pressure the glasses exert on the skin, and connected to LCR meter (E4980AL, Keysight) to record the real-time variation of capacitance for one minute. The capacitance could be converted to absolute pressure (mmHg) according to the calibration of the sensor. The pressure data acquired were used to identify the sensing location in the Results Fig.3.

C. Volunteer Test

The study was approved by the Institutional Review Board (IRB) at the Shenzhen Institute of advanced technology, Chinese Academy of Sciences (approval number: siat-irb-190715-h0367). All participants were informed of the agreement in advance.

Durability test

In the test, a volunteer wore the blink-sensing glasses during normal daily activities. The test started at 9 a.m. and ended at 6 p.m. In addition, to verify whether the glasses were affected by

ambient light, volunteers were asked to sit in a dark office without lights for 20 minutes. All the data were cut into segments of every 30 seconds. Within each 30 seconds, if there was a blink signal that can be recognized artificially, the 30 seconds was labeled as the effective time. Otherwise, it was considered invalid. In the literature of signal quality assessment, artificial judgment was regarded as the gold standard (Liu, C., 2011; Langley, P., 2012; Moody, B. E., 2011). The whole process was judged manually, and there was no error caused by algorithm processing.

Accuracy test

Four volunteers participated in the accuracy test. Every volunteer worked with a computer in the office, wore blinking-sensing glasses to detect blinking, and used a camera (C270i IPTV, Logitech) to record blink synchronously.

Dry eye test

In the dry eye test, firstly, volunteers were randomly recruited from the population to fill out the OSDI scale. The OSDI scale (ocular surface disease index scale) was the most common used questionnaire for clinical diagnosis of dry eye, mainly used for the initial diagnosis of dry eye and evaluation of the severity of the disease (Penny A., 2011). According to the standard of OSDI (Kazuo, T., 1998), the subjects can be divided into the healthy group (score less than or equal to 12) or the dry eye group (score greater than 12). Then, subjects in both groups were asked to wear the blink-sensing glasses and watch the same video for 10 minutes in a properly controlled environment (i.e., in an office). The data collected by blink-sensing glasses were used in the analysis of blink features of patients with dry eye.

D. Template generation

In the blink detection section, a typical template of the blink pattern is prepared in advance, generated from the simultaneous recordings of the pressure and the video signals for two hours. The two hours of data consisting of 10 minutes of data from each of 12 volunteers are used to form the template. Specifically, the key features, including the start, the end, and the peak of each blink pattern are marked in the pre-processed pressure signal, according to the video labeling. Next, the features of blink patterns are counted, and the statistical average blink pattern length (75 points collected at a sampling rate of 125Hz) is used as the template length. On this basis, all blink patterns during two hours are extracted as vectors of 75 elements, and the template is the average of these vectors.

Durability Test Results

In order to further evaluate the long-term performance and the reliability of the blink-sensing glasses in actual scenarios with various daily activities, the durability test of the device was carried out for up to 9 hours continues recording. The test and computational details were in the **Transparent Method.**

Table S3 The durability test results. Related to Table 1.

Test period	Activities during this time	Effective time	Effective time ratio
9:30 am-11:30 am	Read paper and code	117 min 30 s	97.92%
11:30 am-1:00 pm	Eat lunch and talk	77 min	85.56%
1:00 pm-1:30 pm	The volunteer took off her glasses for a nap. The device is in operation but cannot count the effective time		
1:30 pm-2:00 pm	be in a daze, chat with colleagues	28 min 30 s	95.00%
2:00 pm-3:50 pm	Process data and code	109 min 30 s	99.55%
3:50 pm-4:30 pm	Watch videos and walk around the office	38 min	95%
4:30 pm-5:55 pm	Work and play phone	84 min	98.80%
8:00 pm-8:20 pm	sit in office without lights on	20 min	100%

As can be seen from **Table S3**, the effective time referred to the time that the blink event waveform was not submerged in the noise of the original signal, and was often calculated in the study of signal quality assessment (Moody, B. E., 2011). Effective time ratio was the ratio of effective time to test time. In the working scenarios, the glasses could stably collect the signals including blink events, and the effective time ratio was more than 95% in all three time periods of 9:30am-11:30am, 2:00pm-3:50pm, 4:30pm-5:55pm. The effective time ratio decreased significantly from 11:30am to 1:00pm and returned after 1:30pm, indicated that eating might have a great impact on the effective signal acquisition. The speculate reason may lie in that the muscles around the mouth moved in eating activities, and the levator muscles of the upper lip and the alar that were connected to the orbicularis oculi also moved in a large range, which caused interference to the signal. Secondly, when eating, the head moved frequently, which may hide the tight fit between the sensor and the skin, resulting in poor acquisition of the blink signal. Seen from the effective time ratio from 3:50pm-4:30pm, normal walking hardly impacted on the effective signals acquisition.

Moreover, the effective time ratio was 100% in the period of 8:00pm-8:20pm, which indicated that the ambient light did not affect the signal acquisition.

Supplemental References

Liu, C., Li, P., Zhao, L., Liu, F., & Wang, R., (2011). Real-time signal quality assessment for ECGs collected using mobile phones. *Computing in Cardiology. IEEE.*

Langley, P., Marco, L. Y. D., King, S., Duncan, D., & Murray, A., (2012). An algorithm for assessment of quality of ECGs acquired via mobile telephones. *Computing in Cardiology. IEEE.*

Moody, B. E., (2011). Rule-based methods for ECG quality control. *Computing in Cardiology, 2011. IEEE.*

Penny A., Asbell, F.J., Stapleton, K.W., Esen, K., Akpek, P.A., Reza D., et al., (2011). The International Workshop on Meibomian Gland Dysfunction: Report of the Diagnosis Subcommittee. *Investigative Ophthalmology & Visual ence, 52(4):2006-49.*

Kazuo, T., (1998) Tear dynamics and dry eye. Progress in Retinal & Eye Research, 17(4):565.